Method of Extracting Solar Cell Parameters From Derivatives of Dark *I–V* Curves

Brett J. Hallam, Phill G. Hamer, Ruy S. Bonilla, Stuart R. Wenham, and Peter R. Wilshaw

***Abstract*—A method is presented to extract solar cell parameters from the derivatives of dark current–voltage curves with a three-diode model, using the monotonic properties of the current–voltage characteristic associated with each diode or resistive current. The method yields an improved accuracy of the solar cell parameters when compared with that used on the actual current–voltage curves. Despite the complexity of the three-diode model with seven fit parameters, a good accuracy can be reached using the proposed method with a relatively small computational effort. A hypothetical case is presented using various approaches to obtain the solar cell parameters, with a root-mean-square error for the logarithm of the current–voltage curve ($\mathrm{RMS}_{\log_{10} I}$) of 4×10^{-3}. An example fitting is then demonstrated on a multicrystalline passivated emitter rear contact solar cell, yielding $\mathrm{RMS}_{\log_{10} I} = 1.45 \times 10^{-1}$.**

***Index Terms*—Characterization of photovoltaic (PV), curve fitting, PV cells.**

I. Introduction

RECOMBINATION in silicon solar cells significantly affects performance. As solar cell manufacturers push to develop more efficient devices, significant efforts are placed around understanding recombination mechanisms in devices and, importantly, how they can be eliminated. For example, in recent years, several key developments have been used to improve the efficiencies of solar cells. For p-type solar cells, the development of new and improved silver pastes has allowed a shift to more lightly doped emitters. This has resulted in a decrease in Auger-related emitter recombination components and an improvement in the blue response, while enabling a low-resistance ohmic contact and effective shielding of minority carriers from the metal/silicon interface [1]. Another key development is the transition to the passivated emitter and rear locally contacted (PERC) solar cell [2], [3], by passivating the rear surface of the solar cell and using localized rear contacts rather than a full-area aluminum back-surface field. This reduced contact fraction has the benefit of improving rear surface passivation and, therefore, decreasing dark saturation current densities. However, the use of localized rear contacts increases series resistance losses in the device, and the improved rear surface enhances the impact of bulk defects. As a result, methods to eliminate the negative impact of bulk defects have become increasingly important, which has seen a rapid development of engineering methods such as advanced illuminated hydrogen passivation processes to reduce the impact of defects. For example, rapid treatments performed on finished screen-printed solar cells have been used for the passivation of boron–oxygen defects in Czochralski silicon or defect clusters in multicrystalline silicon [4]. For n-type silicon solar cells, which typically use high-bulk-lifetime wafers, efforts have focused on the implementation of passivated contact structures to improve surface passivation [5], [6].

A number of characterization techniques are commonly used throughout solar cell fabrication including photoluminescence imaging [7] and photoconductance lifetime measurements [8]. On finished devices, recombination losses are often quantified using techniques such as photoluminescence imaging and current–voltage (*I–V*) measurements. For *I–V* measurements, several methods can be utilized such as illuminated *I–V* measurements, as well as that performed under open-circuit conditions (Suns–V_{OC}) to remove series resistance effects [9], or dark *I–V* measurements to remove light-generated current effects. In this work, we focus on the use of dark *I–V* measurements. Dark *I–V* curves provide significant detail about the various recombination losses in solar cells. For example, providing information about series and shunt resistance mechanisms, as well as dark saturation current densities and resistance-limited recombination mechanisms in the device. A thorough study of dark *I–V* curves with the associated recombination losses and understanding of such losses was presented by McIntosh [10]. By knowing the performance-limiting recombination mechanisms in a device, processes can be modulated to reduce or eliminate such recombination mechanisms.

A variety of methods have been used to fit *I–V* curves, such as the Newton–Raphson technique, although particular attention must be paid to the initial conditions to ensure convergence of the iteration and a high level of accuracy of the determined values [11]. Other methods have included the use of algorithms to find the root of a function of voltage and current ($f(V, I)$) that is equal to zero for only the correct value of I [12], genetic

Manuscript received May 19, 2017; revised June 30, 2017; accepted July 18, 2017. Date of publication August 2, 2017; date of current version August 18, 2017. This work was supported in part by the Australian Government through the Australian Renewable Energy Agency and the Australian Centre for Advanced Photovoltaics, and in part by the U.K. Government through the International and Industrial Engagement Fund and the Supersilicon project (EP/M024911/1), supported by the Engineering and Physical Sciences Research Council. *(Corresponding author: Brett J. Hallam.)*

B. J. Hallam and S. R. Wenham are with the School of Photovoltaic and Renewable Energy Engineering, University of New South Wales, Kensington, NSW 2052, Australia (e-mail: brett.hallam@unsw.edu.au; s.wenham@unsw.edu.au).

P. G. Hamer, R. S. Bonilla, and P. R. Wilshaw are with the Department of Materials, University of Oxford, Oxford OX1 2JD, U.K. (e-mail: phillip.hamer@materials.ox.ac.uk; sebastian.bonilla@materials.ox.ac.uk; peter.wilshaw@materials.ox.ac.uk).

Color versions of one or more of the figures in this paper are available online at http://ieeexplore.ieee.org.

Digital Object Identifier 10.1109/JPHOTOV.2017.2731778

algorithms, and particle swarm optimizations [13], [14], as well as various iteration and estimation methods [15]–[19]. This paper will discuss a method to extract information on the solar cell parameters in the three-diode model from the derivatives of dark *I–V* curves. It will compare various approaches with different assumptions for the extraction of the parameters and discuss the limitations of each approach. It will demonstrate that despite the complexity of the three-diode model, a good accuracy can be achieved with a relatively simple procedure and small computational effort.

II. One-Diode, Two-Diode, and Three-Diode Models

To fit illuminated *I–V* or dark *I–V* curves, various equivalent circuit models may be used, with different numbers of diodes. In a one-diode model, the dark saturation current components that represent the various recombination mechanisms in the device are lumped together into a single diode D_1, with current I_1 and associated dark saturation current density of I_{0_1}. This diode has a floating ideality factor, n_1. Series resistance R_S effects are also lumped together, acting on the total current I of the device. Similarly, shunting effects are lumped together into a single parallel resistance R_{SH} with associated current I_{SH}. In many instances, this fitting fails to accurately describe the dark *I–V* curves of a solar cell, and as a result, a poorly modeled fit is obtained.

In the two-diode model, in addition to R_S and R_{SH}, two separate diodes are used to represent recombination in the device. For the first diode, D_1, an ideality factor of unity is assumed ($n_1 = 1$). The dark saturation current density associated with this diode (I_{0_1}) represents the current crossing the p-n junction from recombination in the bulk, emitter, and surfaces of the device. This includes both Shockley–Read–Hall (SRH) [20], [21] and Auger recombination effects, giving a current flowing through diode D_1 of I_1. The second diode D_2 has a floating ideality factor, n_2. The dark saturation current density associated with this diode (I_{0_2}) can be caused by SRH recombination in the depletion region [22], SRH recombination at the edge [23], where the edge intersects the p-n junction, and SRH recombination in high-injection conditions [24]. This gives a current I_2 flowing through D_2. Similarly, in many instances, the two-diode model is not able to provide an accurate representation of the dark *I–V* characteristics of a solar cell.

In the three-diode model, an additional diode is present. The current I_H flowing through this third diode D_H is used to represent resistance-limited enhanced recombination in the device, with resistance R_H, due to localized recombination [10], [25]. Here, D_H has a floating ideality factor, n_H. In the three-diode model, D_1 and D_2 have fixed ideality factors of $n_1 = 1$ and $n_2 = 2$, respectively. The electrical circuit used to describe solar cells for the three-diode model is shown in Fig. 1, including the light-generated current I_L (shown in gray) that is zero for dark *I–V* curves. The equivalent circuit for the one-diode model can be obtained by ignoring current paths I_2 and I_H, and similarly for the two-diode model by ignoring the current path I_H.

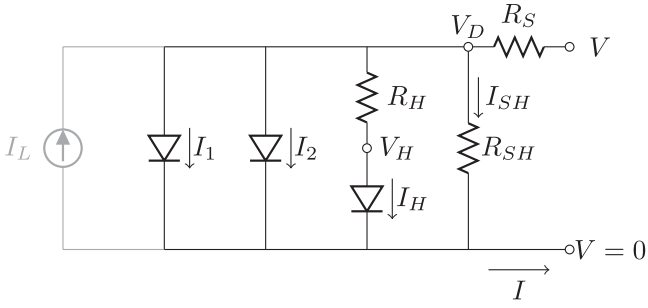

Fig. 1. Circuit diagram for the three-diode model of a solar cell.

III. Challenges of Plotting *I–V* Curves and Fitting Dark *I–V* Data

There are significant challenges in extracting appropriate solar cell parameters from dark *I–V* data: first, the low signal-to-noise ratios, particularly for values in the vicinity of $V = 0$ V that are required for extracting some parameters; second, the diode models used are only theoretical constructions to approximate the recombination behavior of solar cells. However, they do not fully describe the complicated behavior of silicon solar cells. A third major challenge is the complicated nature of the mathematics used in these diode models. There is even a challenge in being able to plot modeled *I–V* curves to enable curve fitting. For isolated components, *I–V* curves can be plotted easily from an explicit function of the current through each component in terms of the voltage across it, and the associated parameters, to give $I = f(V)$. However, for the given circuit in Fig. 1, the current flowing through each component cannot be expressed by a function only including the cell voltage V and the component parameters. That is, a simple relationship of $I = f(V)$ cannot be found. The currents I_1, I_2, and I_{SH} are directly dependent on the voltage across the component V_D rather than on V. To express the currents as a function of V, knowledge of the total current flowing through the cell (I) and the series resistance (R_S) values is required. Similarly, for I_H, the current directly depends on V_H rather than V or V_D, and hence, knowledge of all current components is required. The equations for the total current through the cell in the dark (neglecting I_L), the current through each component, and the simplifications that can be made for the voltage across the component of either V_D or V_H are shown in (1)–(7), where V_T is the thermal voltage

$$I = I_1 + I_2 + I_H + I_{SH} \tag{1}$$

$$I_1 = I_{0_1}\left(e^{\frac{V - I\cdot R_S}{V_T}} - 1\right) \tag{2}$$

$$I_2 = I_{0_2}\left(e^{\frac{V - I\cdot R_S}{2V_T}} - 1\right) \tag{3}$$

$$I_H = I_{0_H}\left(e^{\frac{V - I\cdot R_S - I_H\cdot R_H}{n_H V_T}} - 1\right) \tag{4}$$

$$I_{SH} = \frac{V - I\cdot R_S}{R_{SH}} \tag{5}$$

$$V_D = V - I \cdot R_S \tag{6}$$

$$V_H = V - I \cdot R_S - I_H \cdot R_S. \tag{7}$$

While an explicit function, $I = f(V)$, cannot be used, the values of I at each given V can be obtained using iterative methods, which can then enable plotting. Given that dark *I–V* curves are monotonically increasing, only one value exists for when the function I equals the input guess for the current (I_{guess}) at a given voltage. Hence, I_{guess} can be varied until it is consistent with the output current determined from the expression of I. Alternatively, explicit expressions of current can be obtained as a function of V_D for I_1, I_2, and I_{SH}, and of V_H for I_H. The corresponding values of I_H at each V_H can then be interpolated to obtain the corresponding value of I_H at V_D. Subsequently, the currents of all components can be added to determine I and then the function interpolated to find the corresponding I values for each cell voltage V. Other methods have used the Lambert W function [26]–[29], although this approach is not straightforward.

There are also significant challenges in fitting dark *I–V* curves due to the number of variables. In the three-diode model, there are seven variables. Fitting such curves with potentially hundreds of points by sweeping each variable and establishing a least-squares fit can be quite computationally expensive. Even, with approximate values of R_{SH} and R_S, five variables remain to fit in the three-diode model.

Similarly, expressions of the derivatives of each current component cannot be expressed in terms of only V, but also require values for I and the total derivative ($\frac{dI}{dV}$). The equations for the derivatives of each current component using the chain rule and are shown in (8)–(12). Again, iterative methods can be used to plot curves of $\frac{dI}{dV}$. Alternatively, the derivative can be obtained numerically from the function of I by determining the local gradient at each point. This appears to be a simpler solution and is the approach used in this work

$$\frac{dI}{dV} = \frac{dI_1}{dV} + \frac{dI_2}{dV} + \frac{dI_H}{dV} + \frac{dI_{SH}}{dV} \tag{8}$$

$$\frac{dI_1}{dV} = \frac{I_{0_1}}{V_T} e^{\frac{V_D}{V_T}} \cdot \left(1 - \frac{dI}{dV} R_S\right) \tag{9}$$

$$\frac{dI_2}{dV} = \frac{I_{0_2}}{2V_T} e^{\frac{V_D}{2V_T}} \cdot \left(1 - \frac{dI}{dV} R_S\right) \tag{10}$$

$$\frac{dI_H}{dV} = \frac{I_{0_H} e^{\frac{V_H}{n_H V_T}}}{n_H V_T + I_{0_H} e^{\frac{V_H}{n_H V_T}}} \cdot \left(1 - \frac{dI}{dV} R_S\right) \tag{11}$$

$$\frac{dI_{SH}}{dV} = \frac{1}{R_{SH}} \cdot \left(1 - \frac{dI}{dV} R_S\right). \tag{12}$$

IV. Fitting Dark *I–V* Curves Using Derivatives

A significant amount of information about component parameters is given in the curve of $\frac{dI}{dV}$. An example theoretical curve of the magnitude of I ($\mid I \mid$) is shown in Fig. 2 along with the derivative of I, $\frac{dI}{dV}$. It is noted that for $V < 0$ V, $I < 0$ A, and therefore, plotting $\mid I \mid$ when using a logarithmic scale is helpful for establishing the fit to I at negative voltages. In this example,

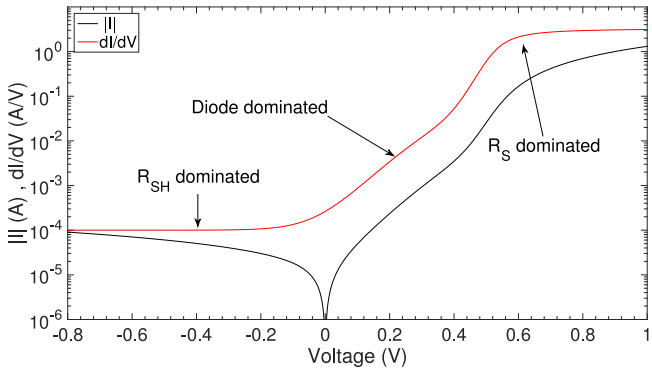

Fig. 2. Simulated dark *I–V* curve (absolute value) and associated $\frac{dI}{dV}$ curve for a sample with the following parameters: $I_{0_1} = 800$ fA, $I_{0_2} = 5 \times 10^{-7}$ A, $R_S = 0.3\,\Omega$, $R_{SH} = 10\,000\,\Omega$, $I_{0_H} = 1 \times 10^{-5}$ A, $R_H = 30\,\Omega$, and $n_H = 2.5$.

the $\frac{dI}{dV}$ curve is dominated by R_{SH} effects for $V < -0.2$ V. At high voltages ($V > 0.8$ V), the curve is dominated by R_S effects. In the intermediate regions transitioning from the R_{SH} dominated region to the R_S dominated region ($0.2\text{ V} < V < 0.8\text{ V}$), the curve is dominated by the three diodes. Depending on the parameters of an individual sample, these ranges will vary. For example, in heavily shunted samples (with sufficiently low values of R_{SH} in relation to the diode components,) R_{SH} will dominate to higher V and possibly still dominate for voltages in the vicinity of $V = 0$ V or slightly above.

Curves of $\frac{dI}{dV}$ provide valuable information about the solar cell parameters and can be used to place limits of the range of values a given solar cell parameter can take. With the monotonic increase of all current contributions, the benefit of using derivatives is that tighter tolerances can be placed on the values rather than directly using *I–V* curves.

To demonstrate this method, we will first fit hypothetical *I–V* data, followed by experimental data later in the paper. For the theoretical example in the following sections, we use hypothetical *I–V* and $\frac{dI}{dV}$ curves of a cell with the following parameters: $I_{0_1} = 800$ fA, $I_{0_2} = 5 \times 10^{-7}$ A, $R_S = 0.3\,\Omega$, $R_{SH} = 10\,000\,\Omega$, $I_{0_H} = 1 \times 10^{-5}$ A, $R_H = 30\,\Omega$, and $n_H = 2.5$. In the following simulations, these curves of *I–V* and $\frac{dI}{dV}$ will be referred to as the actual *I–V* and $\frac{dI}{dV}$ curves. Simulated curves used to predict parameters for the cell will be referred to as modeled curves. For this, voltages are in the range of $-0.8\text{ V} < V < 1\text{ V}$ with 100 data points.

A summary of the fitting procedure used in this work is shown diagrammatically in Fig. 3. It highlights the range of voltages, V_{range}, used to determine each given parameter. This diagram is here to guide the reader through the following sections. Unless otherwise specified, once an initial value for a given parameter has been estimated, the parameter remains enabled for the determination of other parameters.

It should be noted that although the three-diode model is used in this paper to demonstrate the method, the method is also applicable for the one-diode and two-diode models. However, appropriate changes must be made in the determination of I_{0_1}

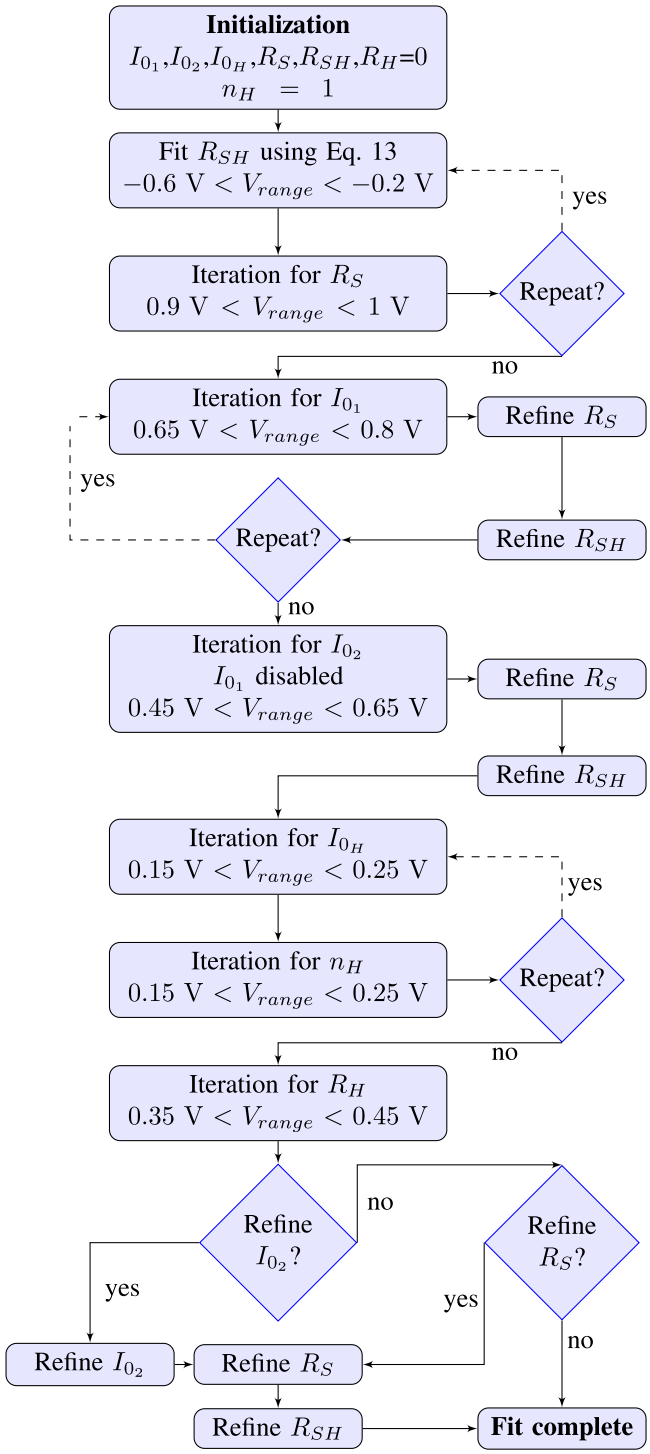

Fig. 3. Summary of the iterative fitting procedure for dark *I–V* data. All parameters are enabled unless otherwise specified.

and/or I_{0_2} to allow for floating ideality factors, such as for the determination of I_{0_H} in the three-diode model.

A. Fitting the Shunt Resistance (R_{SH})

Extracting the shunt resistance is relatively straightforward. At sufficient reverse biases, the exponential terms for the currents flowing through diodes D_1, D_2, and D_H are zero, and hence, there is a constant reverse current component flowing through the three diodes of $I_{\text{reverse}} = I_{0_1} + I_{0_2} + I_{0_H}$. Subsequently, there is no contribution of the diode currents to $\frac{dI}{dV}$. In this regime, $\frac{dI}{dV}$ is dominated by R_{SH}, with only a minor influence of R_S. It should be noted, however, that care must be taken not to use excessively high reverse biases for R_{SH} extraction, where the potential reverse breakdown effects could affect the accuracy of the value obtained. The shunt conductance (G_{SH}) can then be taken as an average values of $\frac{dI}{dV}$ over a given range, for example, between -0.6 V $< V <$ -0.2 V. As a first approximation, R_{SH} can be approximated as the inverse of G_{SH}. In Fig. 4, G_{SH} is estimated as 1.012×10^{-4} S, corresponding to an estimate for R_{SH} of 9.89×10^3 Ω, with $<1.2\%$ error. However, once knowledge about R_S is available, it should be corrected for R_S, particularly when R_S is high. The equation for determining R_{SH} is given as

$$R_{SH} = \frac{(1 - G_{SH} \cdot R_S)}{G_{SH}}. \tag{13}$$

If taking an estimate of R_{SH} at $V = 0$ V, the influence of D_2 and D_H will result in an overestimation of the value for G_{SH}, with a value of 2.67×10^4 S. This would result in an estimate of R_{SH} of 3.75×10^3 Ω, which is a 167% underestimation of the actual value. However, with a reduced influence of D_2 and D_H (such as a reduction of one order of magnitude for I_{0_2} and I_{0_H}), this would be reduced to an underestimation in R_{SH} of 14.3%. For a two order of magnitude reduction in I_{0_2} and I_{0_H}, the underestimation in R_{SH} would be reduced to 1.6%. Similarly, reduced values of I_{0_2} and I_{0_H} would result in improved estimations of the R_{SH} when taking an approximation from the average value of $\frac{dI}{dV}$ in the range between -0.6 V $< V <$ -0.2 V.

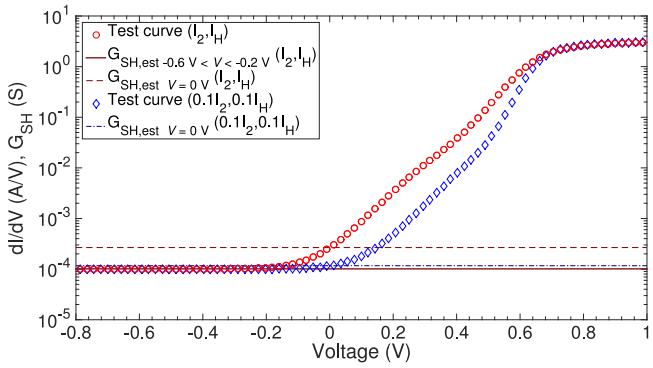

Fig. 4. Simulated $\frac{dI}{dV}$ curve for a sample with the values specified in Fig. 2 (I_2 and I_H) or a one order of magnitude reduction to the values of $I_{0_2} = 5 \times 10^{-8}$ A and $I_{0_H} = 1 \times 10^{-6}$ A ($0.1I_2$ and $0.1I_H$). Values for the estimated shunt conductance $G_{SH,\text{est}}$ are shown for the range of -0.6 V $< V <$ -0.2 V (for I_2 and I_H) and at $V = 0$ V for both cases.

B. Fitting the Series Resistance (R_S)

Similarly, a first approximation for R_S can be obtained from the inverse of $\frac{dI}{dV}$ at high voltages. However, doing so overestimates R_S and should be treated as an upper limit of the possible

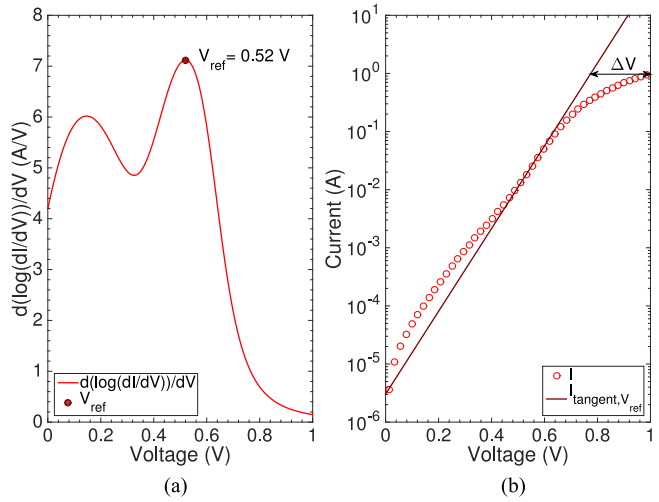

Fig. 5. (a) Curve of $\frac{d\left(\log\left(\frac{dI}{dV}\right)\right)}{dV}$ and the voltage ($V_{\text{ref}} = 0.52$ V) corresponding to the onset of visible resistive effects. (b) Test *I–V* curve and corresponding tangent (on a logarithmic scale) from V_{ref}.

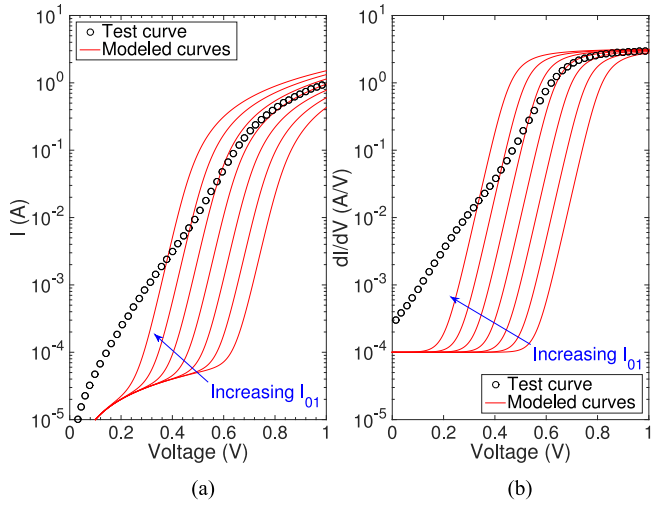

Fig. 6. (a) Test dark *I–V* curve and (b) associated $\frac{dI}{dV}$ curve for a cell with the following parameters: $I_{0_1} = 800$ fA, $I_{0_2} = 5 \times 10^{-7}$ A, $R_S = 0.3\ \Omega$, $R_{SH} = 10\,000\ \Omega$, $I_{0_H} = 1 \times 10^{-5}$ A, $R_H = 30\ \Omega$, and $n_H = 2.5$. Modeled curves in both (a) and (b) show corresponding curves with R_{SH} and R_S enabled (same values), I_{0_2} and I_{0_H} disabled (set to 0), and various I_{0_1} values increasing by a factor of 10 from 1×10^{-15} to 1×10^{-9} A.

R_S values, as it does not take into account any influence of D_1, D_2, and D_H in increasing the $\frac{dI}{dV}$. In this example, a value of $R_S = 0.32\ \Omega$ was obtained, an overestimation of R_S by approximately 6.6%. A lower bound value may be obtained by identifying the voltage at which resistive effects are clearly noticeable in $\frac{dI}{dV}$. In this instance, the monotonically increasing properties of both I and $\frac{dI}{dV}$ are utilized. In the absence of R_S, any change from a domination of D_2 toward D_1 with increasing voltage will increase the slope of the curve $\log\left(\frac{dI}{dV}\right)$, $\left(\frac{d\left(\log\left(\frac{dI}{dV}\right)\right)}{dV}\right)$. Any decrease in the slope of $\log\left(\frac{dI}{dV}\right)$ at high voltages is characteristic of a resistive effect. Therefore, the point at which $\frac{d\left(\log\left(\frac{dI}{dV}\right)\right)}{dV}$ begins to decrease indicates a point at which R_S effects can be observed in the *I–V* curve [see Fig. 5(a)], in this instance corresponding to a reference voltage of $V_{\text{ref}} = 0.52$ V. A tangent (on a logarithmic scale) is then drawn on the *I–V* curve from this point up to a predetermined current value [see Fig. 5(b)]. From this, the difference in voltage (ΔV) between the actual *I–V* measurement and the tangent can be used to estimate R_S. Using this approach, a lower bound value for R_S of 0.25 Ω is obtained (a 17.3% underestimation).

An improved approximation for the R_S can be obtained by simulating the $\frac{dI}{dV}$ for a curve with only R_{SH} and a large value of I_{0_1} active that grossly overestimates a reasonable value of I_{0_1} such as 1×10^{-9} A. Then, an iteration can be performed for curves with various R_S values until a fit to the $\frac{dI}{dV}$ at high voltages (e.g., at $V = 1$ V) is obtained. This can also be considered as an upper limit for R_S. The advantage of using the derivative to form the fit, rather than using the actual *I–V* curve, is highlighted in Fig. 6. When simulating an *I–V* curve using the correct values for R_{SH} and R_S, varying the I_{0_1} value can lead to substantial changes in the value of I at $V = 1$ V. In contrast, the same changes do not significantly affect $\frac{dI}{dV}$. Similarly, a lower limit on the R_S value can be obtained by applying the same test with a sufficiently small I_{0_1} value such as 1×10^{-15} A.

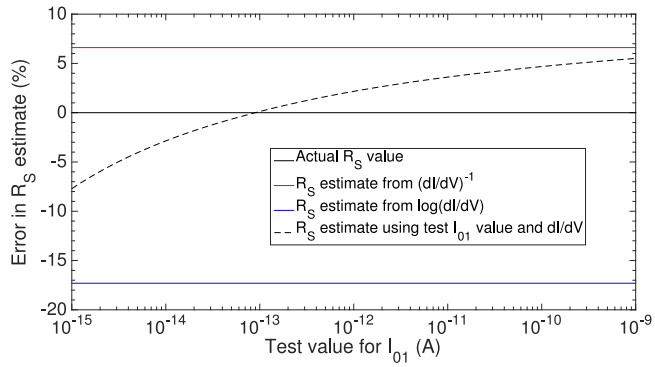

Fig. 7. Upper and lower bounds on R_S values and error in R_S using test values for I_{0_1} for iterations to calculate R_S with only R_{SH}, R_S and I_{0_1} enabled. $R_{SH} = 10\,000\ \Omega$.

Performing such an iteration will, therefore, lead to reduced errors in the obtained upper limit value of R_S, provided that the I_{0_1} value used is sufficiently high. Fig. 7 shows the errors from this R_S extraction by choosing different I_{0_1} values from the test curve shown in Fig. 6. Using a test I_{0_1} value of 1×10^{-9} A results in an overestimation of R_S by 5.5%, to give a value of 0.3165 Ω. Further improvements in the accuracy of R_S can be obtained once approximate values of I_{0_1} and I_{0_2} are known.

C. Fitting I_{0_1} and I_{0_2}

First approximations for the values of I_{0_1} and I_{0_2} can be obtained in a similar manner, which can also be considered as upper limits for the respective values, provided that the R_S is not too high. If the R_S is too high, resistive effects will dominate at large positive biases and result in a slight underestimation of I_{0_1}. To estimate I_{0_1}, only R_S, R_{SH}, and I_{0_1} are enabled,

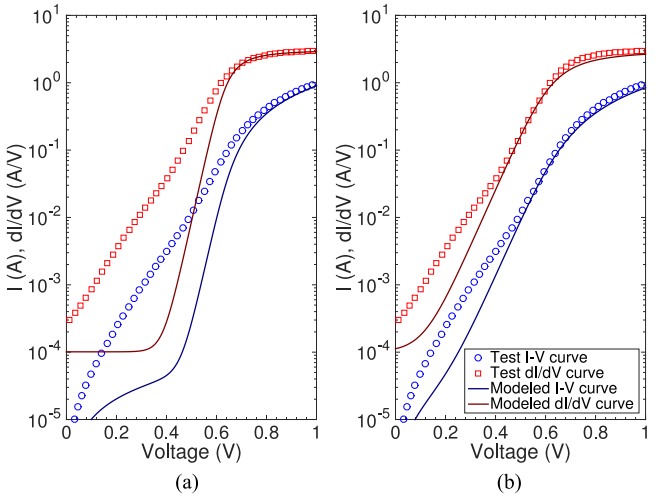

Fig. 8. *I–V* and $\frac{dI}{dV}$ curves, along with modeled curves with R_S, R_{SH}, and I_{0_1} or I_{0_2} enabled for determining upper bounds for (a) I_{0_1} and (b) I_{0_2}.

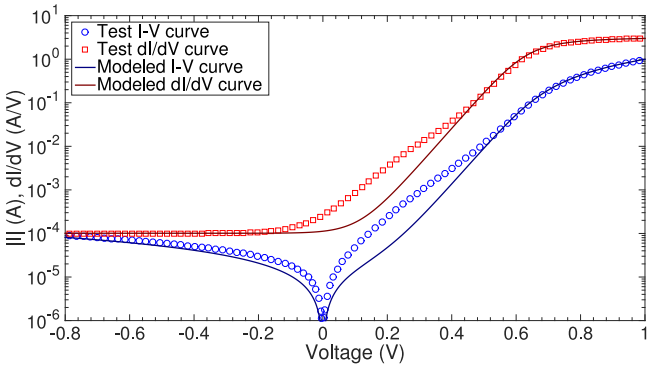

Fig. 9. *I–V* and $\frac{dI}{dV}$ curves along with modeled *I–V* and $\frac{dI}{dV}$ curves using the progressive estimates for R_S, R_{SH}, I_{0_1}, and I_{0_2}.

using the current estimates of R_S and R_{SH}. An iteration is performed to give the highest possible value of I_{0_1} such that the modeled $\frac{dI}{dV}$ curve does not exceed the value of the actual $\frac{dI}{dV}$ curve at any point within a specific range (e.g., a high positive bias range from 0.4 V $< V <$ 1 V). The same method is then used to determine an upper limit of I_{0_2} by disabling I_{0_1} and enabling I_{0_2}. Example fittings for the upper limits of I_{0_1} and I_{0_2} are shown in Fig. 8. The images also show the corresponding values of the modeled and actual *I–V* curves, highlighting the underestimation of the *I–V* curve. Therefore, if performing the same iteration against the *I–V* curve rather than the $\frac{dI}{dV}$ curve, it will result in a larger error in I_{0_1} and I_{0_2}. Here, extracting values from the $\frac{dI}{dV}$ curve result in an estimation for I_{0_1} of 8.81 fA and I_{0_2} of 5.83×10^{-7} A, overestimating the respective values by 10.1% and 16.5%. In comparison, extracting the values from the *I–V* curve results in estimations of $I_{0_1} = 243$ fA (203% overestimation) and 6.45×10^{-7} A (29% overestimation).

Once approximate values of I_{0_1} and I_{0_2} are known, an accurate value of R_S can be obtained. This value is obtained using the same method as used previously to determine R_S, with both I_{0_1} and I_{0_2} enabled using the current estimates of I_{0_1} and I_{0_2}. Here, despite the errors in the estimations of I_{0_1} and I_{0_2}, an error in R_S of less than 0.1% is obtained. It should be noted, however, that for excessively high values of R_S, knowledge of approximate values for D_H may be required for an accurate estimation of R_S. Using the estimations of the values obtained so far, an excellent fit can be obtained for large positive biases dominated by D_1, D_2, and R_S effects. The dominant errors in the fit arose from the presence of D_H associated recombination (shown in Fig. 9). The corresponding root-mean-squared error of I, i.e., $\text{RMS}_{\log_{10} I}$, is 0.269.

D. Fitting I_{0_H}, n_H, and R_H

Fitting values for the three parameters related to D_H are more involved. However, the values of I_{0_H} and n_H can be estimated in the vicinity of $V = 0$ V, where the resistive effects from R_H can be ignored. Here, in the vicinity of $V = 0$ V, $\frac{dI}{dV}$ is dominated by the D_H, provided that R_{SH} is sufficiently high. If so, then $\frac{dI}{dV}$ is approximately proportional to $\frac{I_{0_H}}{n_H V_T}$. Furthermore, the second derivative is approximately proportional to $\frac{I_{0_H}}{(n_H V_T)^2}$. Therefore, taking the ratio of the first and second derivatives in the vicinity of $V = 0$ V (such as 0 V $< V <$ 0.2 V) can give the value of $n_H V_T$. In this example, this range of voltages results in a range of n_H values from 2.79 to 4.00 (with a minimum value occurring at $V = 0.147$ V). This minimum value of 2.79 is an overestimation by 11.6%, while the values obtained near $V = 0$ V show larger errors to the presence of shunt resistance. Subsequently, I_{0_H} can be estimated using (14) at this voltage, assuming that R_{SH} and D_H are the only active components. In this instance, a value of 1.37×10^{-5} A is obtained, an overestimation by 37%

$$I_{0_H,\text{estimate}} = \frac{I - \frac{V}{R_{SH}}}{e^{\frac{V}{n_H V_T}} - 1}. \tag{14}$$

To improve the accuracy of the n_H estimate, the effects of both R_S and R_{SH} can be removed from *I–V* and $\frac{dI}{dV}$ curves. Here, V is first corrected for the drop in voltage across R_S to give the corresponding values of V_D [according to (6)]. Subsequently, the current is corrected for R_{SH} using (15). Example *I–V* and $\frac{dI}{dV}$ curves corrected for R_S, and both R_S and R_{SH}, are shown in Fig. 10. Using the ratio of the first and second derivatives of the R_S- and R_{SH}-corrected *I–V* curves, using the same uncorrected voltage range (0 V $< V <$ 0.2 V), n_H values in the range of 2.47 to 2.79. Here, the most accurate values are obtained in the range of 0 V $< V <$ 0.1 V. Assuming $V = 0$ V, a value of 2.47 is obtained (1.3% error) with a corresponding I_{0_H} of 1.07×10^{-5} A (7% error). Alternatively, the R_S- and R_{SH}-corrected *I–V* curve at sufficiently large negative voltages provides the negative summed value of I_{0_1}, I_{0_2}, and I_{0_H}. In Fig. 10, this value is 1.05×10^{-5} A, which provides an estimation of the upper limit of I_{0_H} (a 5.5% overestimation). A lower limit for I_{0_H} is obtained with the knowledge of the upper limits of both I_{0_1} and I_{0_2}. In the situation that $I_{0_H} >> I_{0_1} + I_{0_2}$, this provides a very accurate value for I_{0_H}. Here, a value of $I_{0_H} = 9.47 \times 10^{-6}$ A is obtained, a 5.3% underestimation.

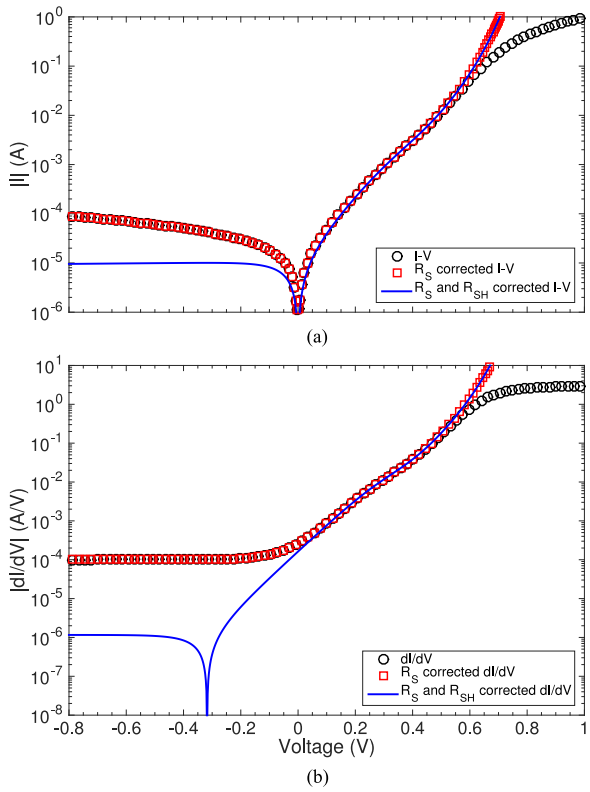

Fig. 10. (a) *I–V* and (b) $\frac{dI}{dV}$ curves along with the corresponding curves corrected for R_S, and both R_S and R_{SH}.

Using these upper and lower limits for I_{0_H} and the known value of I at this voltage, assuming that D_H is the only active component, this gives respective values of 2.46 and 2.40 for n_H, with corresponding errors of 1.6% and 3.8%

$$I_{R_S,R_{SH}\text{-corrected}} = I_{\text{cell}} - \frac{V_D}{R_{SH}}. \tag{15}$$

I_{0_H} and n_H can also be estimated using an iterative approach at low voltages. Here, a voltage range is chosen (such as 0.05 V $< V <$ 0.1 V) that is sufficiently low to ignore effects of R_H. I_{0_H} is estimated using the *I–V* curve. A test curve is generated with current estimates for R_S, R_{SH}, I_{0_1}, and I_{0_2}. For all iterations, the R_H is disabled. In the first iteration, n_H is assumed to be 1. The iteration is performed to find the maximum value of I_{0_H} that results in the modeled curve being less than the actual *I–V* curve for all values in the voltage range. With this value of I_{0_H}, an iteration is performed using $\frac{dI}{dV}$ to find the minimum value of n_H, where the test $\frac{dI}{dV}$ curve is lower than the actual $\frac{dI}{dV}$ curve for all values in the voltage range. This process is performed multiple times to converge on an approximate value of I_{0_H} and n_H. In this instance, a value of $I_{0_H} = 1.071 \times 10^{-5}$ A is obtained, an 7.1% overestimation. The corresponding value of $n_H = 2.67$ is obtained, a 6.9% overestimation. Using the same method of iteration with the estimate of the lower limit of I_{0_H} from the R_S- and R_{SH}-corrected *I–V* curve, n_H is estimated at 2.50, with $<$ 0.1% overestimation.

Subsequently, R_H is estimated using an iterative method to find the minimum R_H value to keep the test $\frac{dI}{dV}$ curve below the actual $\frac{dI}{dV}$ curve over a specified voltage range. Here, I_{0_H} is taken as the lower bound from the R_S- and R_{SH}-corrected *I–V* curve (9.47×10^{-6} A), and n_H is taken from the ratio of the first and second derivatives of the corrected *I–V* curve (2.47). From this iteration, a value of $R_H = 37.0\ \Omega$ is obtained, a 23.4% overestimation of R_H. Despite what may appear as significant errors for some parameters (such as for R_H), the fitted curve provides an excellent approximation of the actual *I–V* curve when presented on a logarithmic scale (not shown), with $\text{RMS}_{\log_{10} I} = 0.012$. The dominant discrepancy of the curves comes from the overestimation of I_{0_2} and R_H.

E. Refinement of Values

Once approximations are known for all values, the estimations for several parameters can be refined. For R_S, while in the given example an improved estimate is not required, for excessively high values of R_S, where D_H has a significant influence in the R_S affected region of the $\frac{dI}{dV}$ curve, improved accuracy of the approximation of R_S can be obtained. For this, an iteration is performed to find the maximum value of R_S given the estimation of all other parameters. In this example, no significant change in R_S (0.2999 Ω) or subsequent change in R_{SH} ($9.89 \times 10^3\ \Omega$) is observed.

In the previous approximation of I_{0_2}, the absence of the contributions of diodes D_1 and D_H to the modeled $\frac{dI}{dV}$ resulted in an overestimation of I_{0_2}. To correct for this, R_S- and R_{SH}-corrected $\frac{dI}{dV}$ curves are generated for the actual $\frac{dI}{dV}$ curve and test curves with only the D_1, D_2, or D_H diodes active [see Fig. 11(a)]. Subsequently, at the voltage whereby the ratio of the D_2-related $\frac{dI}{dV}$ curve to the actual $\frac{dI}{dV}$ curve is maximized (the point whereby I_{0_2} is estimated), the values of all diode-related $\frac{dI}{dV}$ values are estimated. An improved estimated for I_{0_2} is given by (16). Here, the revised estimate for I_{0_2} is 5.10×10^{-7} A, a 2.0% overestimation. In the given example, the voltage range is not sufficiently high to allow for an improved approximation of I_{0_1}, as the R_S- and R_{SH}-corrected $\frac{dI}{dV}$ curves of the actual $\frac{dI}{dV}$ curve and D_1-related curve did not converge

$$I_{0_2,\text{revised}} = I_{0_2} \frac{\frac{dI_{0_2}}{dV}}{\frac{dI_{0_1}}{dV} + \frac{dI_{0_2}}{dV} + \frac{dI_{0_H}}{dV}}. \tag{16}$$

Subsequently, I_{0_H} can be revised using the updated value of I_{0_2} to give $I_{0_H} = 9.55 \times 10^{-6}$ A, a 4.5% underestimation. Then, the value of n_H can be obtained from an iteration of $\frac{dI}{dV}$ as used previously to give a value of $n_H = 2.46$ (an error of 1.5%), and similarly, R_H can be obtained to give a value of $R_H = 33.7\ \Omega$ (a 12.3% error). These values provide an excellent fit to the $\frac{dI}{dV}$ curve as shown in Fig. 11(b), with $\text{RMS}_{\log_{10} I} = 0.004$.

V. Example Applying the Method to Real Data

An industrial 156 mm $\times$ 156 mm PERC solar cell was cleaved into small cells (3 cm $\times$ 2 cm). The dark *I–V* characteristics were measured on a custom-built *I–V* tester using a Keithley 2401 Source Measuring Unit and four-wire sensing to minimize contributions from resistance in the test leads. An example dark *I–V* curve is shown in Fig. 12(a) along with the

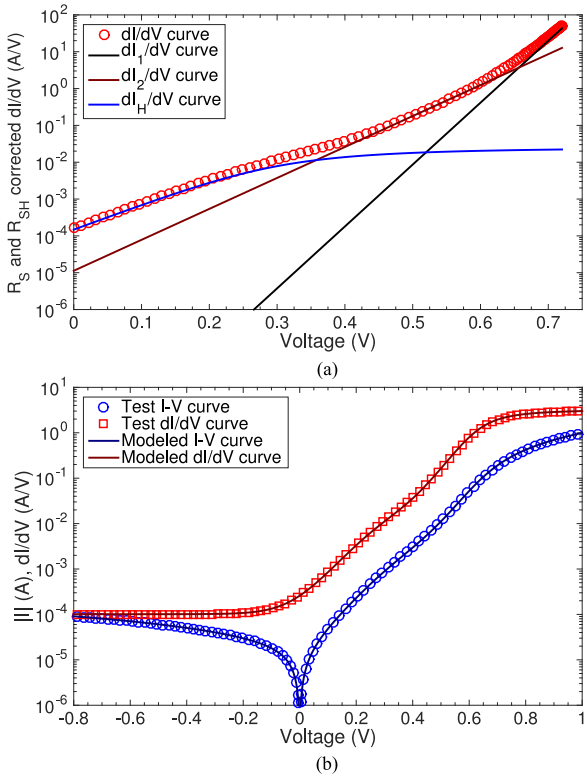

Fig. 11. (a) Actual R_S- and R_{SH}-corrected $\frac{dI}{dV}$ curve and modeled D_1, D_2, and D_H $\frac{dI}{dV}$ curves. (b) Actual *I–V* and $\frac{dI}{dV}$ curves along with the corresponding test curves using the estimated parameters: $I_{0_1} = 881$ fA, $I_{0_2} = 5.11 \times 10^{-7}$ A, $R_S = 0.2999\ \Omega$, $R_{SH} = 10\,000\ \Omega$, $I_{0_H} = 9.99 \times 10^{-6}$ A, $R_H = 34.45\ \Omega$, and $n_H = 2.52$.

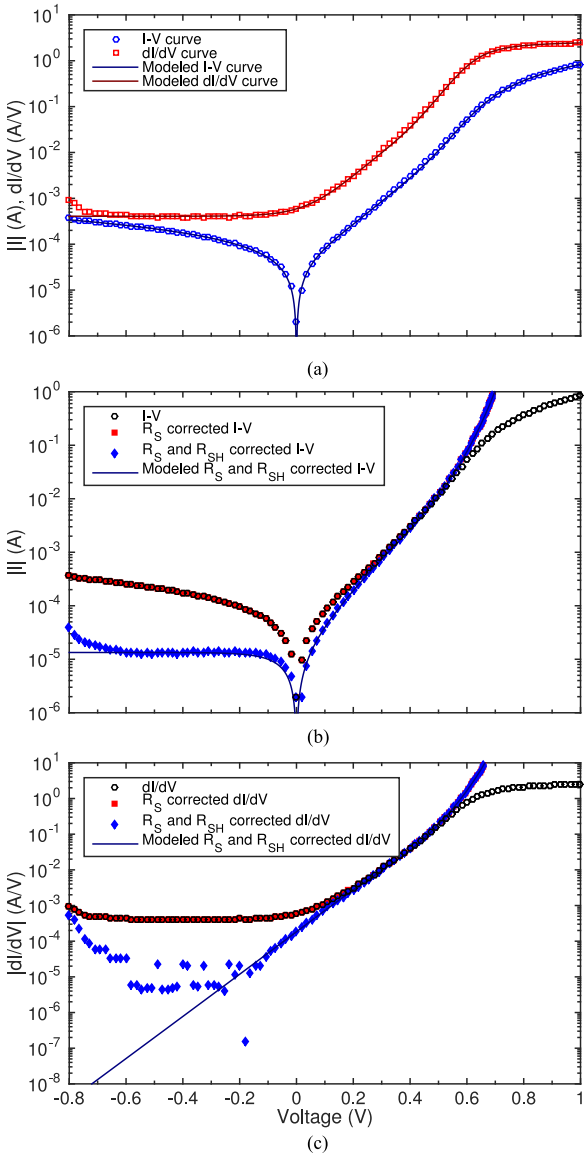

Fig. 12. *I–V* and $\frac{dI}{dV}$ data and the corresponding test curves with the estimated parameters: $I_{0_1} = 1120$ fA, $I_{0_2} = 5.26 \times 10^{-7}$ A, $R_S = 0.370\ \Omega$, $R_{SH} = 2460\ \Omega$, $I_{0_H} = 1.29 \times 10^{-5}$ A, $R_H = 34.8\ \Omega$, and $n_H = 2.85$. Actual (b) *I–V* and (c) $\frac{dI}{dV}$ curves along with the corresponding curves corrected for R_S, and both R_S and R_{SH}.

fitted curve using the methods described in the previous section. As shown, an excellent fit is obtained using the parameters listed in the caption, with an error of $\text{RMS}_{\log_{10} I} = 0.145$. The associated R_S- and R_{SH}-corrected *I–V* and $\frac{dI}{dV}$ curves are shown in Fig. 12(b) and (c), respectively. It should be noted that no smoothing was applied to the data. Although accurate data acquisition is essential to ensure that the background noise in the instrument in the low-current range does not produce significant noise, the application of smoothing will likely improve the quality of the data for fitting purposes.

At voltages below -0.6 V, the actual $\frac{dI}{dV}$ data deviate from the modeled curve due to noise [see Fig. 12(a)]. The associated noise in the R_S- and R_{SH}-corrected *I–V* curve [see Fig. 12(b)] would cause an error in the determination of I_{0_H}. However, the flat nature of the R_S- and R_{SH}-corrected curve in range of $-0.6\ \text{V} < V < -0.2$ V indicates a high accuracy of the determined R_{SH} (2460 Ω), and therefore the estimation of I_{0_H}. This provides an estimation of the summed value of I_{0_1}, I_{0_2} and I_{0_H} of $1.29 - 1.41\ \times 10^{-5}$ A. With the known estimations of I_{0_1} (1120 fA) and I_{0_2} (5.26×10^{-7} A) being substantially lower than this, it accurately estimates I_{0_H}.

One weakness of using $\frac{dI}{dV}$ data for the extraction of solar cell parameters in that small errors in *I–V* data can lead to significant errors in $\frac{dI}{dV}$. This is particularly the case for extremely small currents at negative voltages or in the vicinity of $V = 0$ V. The R_S- and R_{SH}-corrected $\frac{dI}{dV}$ curve in Fig. 12(c) shows noise for $V < -0.1$ V, deviating away from the modeled curve. This suggests that the sensitivity in $\frac{dI}{dV}$ is limited to approximately 1×10^{-5} A/V with this dataset and experimental setup. Hence, for the determination of n_H, the voltage range should be above -0.1 V, but still sufficiently low to avoid significant effects from R_H (or the other diodes). In this example, all data points in the vicinity of $V = 0$ V with currents as low as 1×10^{-6} A resulted in meaningful $\frac{dI}{dV}$ values. The approximation of n_H from the ratio of the R_S- and R_{SH}-corrected curves for *I–V* and $\frac{dI}{dV}$ in the range of $-0.1\ \text{V} < V < 0.1$ V gives a range of $n_H = 2.35$–2.98, compared with a value of 2.85 using an iterative approach.

For the fitted curve in this example, the dominant discrepancy between the actual and modeled *I–V* data is related to

resistance limited recombination effects (D_H). Estimations for the ranges of D_H-related parameters from the iterative processes were $I_{0_H} = 1.28-1.34 \times 10^{-5}$ A, $n_H = 2.83-2.86$, and $R_H = 33.7-36.5\ \Omega$. This entire range of parameters provides an excellent fit to the data with corresponding values for $\mathrm{RMS}_{\log_{10} I}$ in the range of 0.14–0.15.

In our future work, we will apply the technique to a range of *I–V* curves from solar cells with greatly different *I–V* properties. This will serve as further validation for the technique as well as highlighting the associated limitations.

VI. Conclusion

In this paper, a technique to extract recombination and resistance parameters from the derivatives of dark I-V curves has been presented. This method takes advantage of the monotonic properties of each current component and the associated derivative components. To determine R_{SH}, small negative voltages should be used to avoid potential influences of resistance-limited recombination effects from I_{0_H} in the vicinity of $V = 0$ V. For R_S, test curves of $\frac{dI}{dV}$ with a range of I_{0_1} values can be used to give a much closer approximation rather than using $\left(\frac{dI}{dV}\right)^{-1}$ at high voltages. For first approximations of I_{0_1} and I_{0_2}, iterative processes can be applied to find the maximum value at which the simulated $\frac{dI}{dV}$ values are below the actual $\frac{dI}{dV}$ values within in a given voltage range with only the R_{SH}, R_S, and the I_0 component of interest enabled. Subsequently, a more accurate value of R_S can be obtained.

Fitting values for the parameters related to D_H are more involved. The values of I_{0_H} and n_H can be estimated in the vicinity of $V = 0$ V, where the resistive effects from R_H can be ignored. The ratio of the first and second derivatives of the R_S- and R_{SH}-corrected *I–V* curves can be used to obtain the value of n_H and subsequently I_{0_H}. Alternatively, the R_S- and R_{SH}-corrected *I–V* curve can give an upper limit for I_{0_H} as well as a lower limit (based on the upper limit estimations for I_{0_1} and I_{0_2}). Knowledge of I_{0_H} can then be used to refine the estimation of n_H. Another approach is to perform an iteration to determine values of I_{0_H} and n_H in the vicinity of $V = 0$ V. Subsequently, an iterative method is used to determine R_H. Once estimations of all values have been obtained, the same methods can be used to refine the estimations further. On a hypothetical case, a value of with $\mathrm{RMS}_{\log_{10} I} = 0.004$ was obtained demonstrating an excellent fit. The methods were then applied to real *I–V* data from a cleaved industrial PERC solar cell, yielding $\mathrm{RMS}_{\log_{10} I} = 0.145$.

References

[1] V. Shanmugam *et al.*, "Impact of the phosphorus emitter doping profile on metal contact recombination of silicon wafer solar cells," *Sol. Energy Mater. Sol. Cells*, vol. 147, pp. 171–176, 2016.

[2] A. W. Blakers, A. Wang, A. M. Milne, J. Zhao, and M. A. Green, "22.8% efficient silicon solar cell," *Appl. Phys. Lett.*, vol. 55, no. 13, pp. 1363–1365, 1989.

[3] ITRPV Working Group and others, "International technology roadmap for photovoltaics (itrpv.net): Results 2015," *ITRPV: Germany*, 7th ed., 2016.

[4] B. J. Hallam *et al.*, "Advanced hydrogenation of dislocation clusters and boron-oxygen defects in silicon solar cells," *Energy Procedia*, vol. 77, pp. 799–809, 2015.

[5] D. Smith *et al.*, "Generation III high efficiency lower cost technology: Transition to full scale manufacturing," in *Proc. 38th IEEE Photovoltaic Spec. Conf.*, 2012, pp. 594–597.

[6] S. Glunz *et al.*, "The irresistible charm of a simple current flow pattern-25% with a solar cell featuring a full-area back contact," in *Proc. 31st Eur. Photovoltaic Sol. Energy Conf.*, 2015, pp. 259–263.

[7] T. Trupke, R. A. Bardos, M. C. Schubert, and W. Warta, "Photoluminescence imaging of silicon wafers," *Appl. Phys. Lett.*, vol. 89, 2006, Art. no. 044107.

[8] R. A. Sinton, A. Cuevas, and M. Stuckings, "Quasi-steady-state photoconductance, a new method for solar cell material and device characterization," in *Proc. 25th IEEE Photovoltaic Spec. Conf.*, 1996, pp. 457–460.

[9] R. Sinton and A. Cuevas, "A quasi-steady-state open-circuit voltage method for solar cell characterization," in *Proc. 16th Eur. Photovoltaic Sol. Energy Conf.*, 2000, pp. 1–5.

[10] K. R. McIntosh, *Lumps, Humps and Bumps: Three Detrimental Effects in the Current-Voltage Curve of Silicon Solar Cells*. Kensington, Australia: Univ. New South Wales, 2001.

[11] N. Enebish, D. Agchbayar, S. Dorjkhand, D. Baatar, and I. Ylemj, "Numerical analysis of solar cell current-voltage characteristics," *Sol. Energy Mater. Sol. Cells*, vol. 29, no. 3, pp. 201–208, 1993.

[12] S. Suckow, T. M. Pletzer, and H. Kurz, "Fast and reliable calculation of the two-diode model without simplifications," *Prog. Photovoltaics, Res. Appl.*, vol. 22, no. 4, pp. 494–501, 2014.

[13] J. A. Jervase, H. Bourdoucen, and A. Al-Lawati, "Solar cell parameter extraction using genetic algorithms," *Meas. Sci. Technol.*, vol. 12, no. 11, 2001, Art. no. 1922.

[14] M. Ye, X. Wang, and Y. Xu, "Parameter extraction of solar cells using particle swarm optimization," *J. Appl. Phys.*, vol. 105, no. 9, 2009, Art. no. 094502.

[15] K. Ishaque, Z. Salam, and H. Taheri, "Simple, fast and accurate two-diode model for photovoltaic modules," *Sol. Energy Mater. Sol. Cells*, vol. 95, no. 2, pp. 586–594, 2011.

[16] M. G. Villalva, J. R. Gazoli, and E. Ruppert Filho, "Comprehensive approach to modeling and simulation of photovoltaic arrays," *IEEE Trans. Power Electron.*, vol. 24, no. 5, pp. 1198–1208, May 2009.

[17] M. Chegaar, G. Azzouzi, and P. Mialhe, "Simple parameter extraction method for illuminated solar cells," *Solid-State Electron.*, vol. 50, no. 7, pp. 1234–1237, 2006.

[18] A. Ortiz-Conde, F. J. G. Sánchez, and J. Muci, "New method to extract the model parameters of solar cells from the explicit analytic solutions of their illuminated I–V characteristics," *Sol. Energy Mater. Sol. Cells*, vol. 90, no. 3, pp. 352–361, 2006.

[19] M. AlRashidi, M. AlHajri, K. El-Naggar, and A. Al-Othman, "A new estimation approach for determining the I–V characteristics of solar cells," *Sol. Energy*, vol. 85, no. 7, pp. 1543–1550, 2011.

[20] W. Shockley and W. Read, Jr,, "Statistics of the recombinations of holes and electrons," *Phys. Rev.*, vol. 87, no. 5, pp. 835–842, 1952.

[21] R. N. Hall, "Electron-hole recombination in germanium," *Phys. Rev.*, vol. 87, no. 2, p. 387, 1952.

[22] C.-T. Sah, R. N. Noyce, and W. Shockley, "Carrier generation and recombination in pn junctions and pn junction characteristics," *Proc. IRE*, vol. 45, no. 9, pp. 1228–1243, 1957.

[23] C. Henry, R. Logan, and F. Merritt, "The effect of surface recombination on current in $Al_x Ga_{1-x} As$ heterojunctions," *J. Appl. Phys.*, vol. 49, no. 6, pp. 3530–3542, 1978.

[24] W. Shockley, "The theory of p-n junctions in semiconductors and p-n junction transistors," *Bell Syst. Tech. J.*, vol. 28, no. 3, pp. 435–489, 1949.

[25] F. Hernando, R. Gutierrez, G. Bueno, F. Recart, and V. Rodriguez, "Humps, a surface damage explanation," in *Proc. 2nd World Conf. Photovoltaic Sol. Energy Convers.*, 1998, pp. 1321–1323.

[26] J. H. Lambert, "Observationes variae in mathesin puram," *Acta Helvetica*, vol. 3, no. 1, pp. 128–168, 1758.

[27] L. Euler, "De serie lambertina plurimisque eius insignibus proprietatibus," *Acta Acad. Scient. Petropol*, vol. 2, pp. 29–51, 1783.

[28] T. Banwell and A. Jayakumar, "Exact analytical solution for current flow through diode with series resistance," *Electron. Lett.*, vol. 36, no. 4, pp. 291–292, 2000.

[29] A. Jain and A. Kapoor, "Exact analytical solutions of the parameters of real solar cells using lambert w-function," *Sol. Energy Mater. Sol. Cells*, vol. 81, no. 2, pp. 269–277, 2004.

Authors' photographs and biographies not available at the time of publication.